Int. J. Heat Mass Transfer. Vol. 28, No. 11, pp. 2137–2148, 1985
Printed in Great Britain

0017-9310/85 $3.00 + 0.00

Governing equations for heat and mass transfer in heat-generating porous beds—II. Particulate melting and substrate penetration by dissolution*

T. C. CHAWLA,† D. R. PEDERSEN† and W. J. MINKOWYCZ‡

†Reactor Analysis and Safety Division, Argonne National Laboratory, Argonne, IL 60439, U.S.A.
‡Department of Mechanical Engineering, University of Illinois at Chicago, Chicago, IL 60680, U.S.A.

(*Received* 10 *March* 1985 *and in final form* 23 *May* 1985)

Abstract—Upon dryout of the bed, the dominant modes of heat transfer are conduction and radiation. Radiation is modeled through the Rosseland approximation. The melting of stainless-steel particulate imbedded in the fuel is modeled by assuming the bed to be a continuum with conduction and radiation as the dominant modes of heat transfer. The molten steel, after it drains to the bottom of the bed, is assumed to disappear into cracks and mortar joints of the MgO bricks. The melting of fuel in the interior of the bed is modeled identically to the steel particulate, except for the bed settling which is more pronounced in the case of fuel melting and is assumed to be instantaneous owing to the significant weight of overlying bed and sodium pool. The molten layer of fuel, as it collects at the bottom of the bed, causes the heatup of the MgO lining to the eutectic temperature (2280°C), and the MgO lining begins to dissolve. The density gradient caused by the dissolution of MgO leads to natural convection and mixing in the molten layer. The submerged fuel particulate also begins to dissolve in the molten solution and ultimately leads to the conversion of debris to a molten pool of fuel and MgO. The process of penetration of the MgO lining continues until the mixing process lowers the concentration of fuel in the volume of the pool to the level where the internal heat rate per unit volume is not enough to keep the body of the pool molten and leads to freezing in the cooler part of the pool. As the molten pool reaches a frozen or a quiescent state, the MgO brick lining thickness provided is deemed 'safe' for a given bed loading and the external rate of cooling.

INTRODUCTION

IN PART I, we dealt with the phenomena of two-phase flow and boiling in heat-generating fixed porous beds. In Part II, we will analyze the physics of processes that occur subsequent to dryout in the presence of continued internal heating of the bed. To give a better appreciation, we will discuss here the relevent phenomenology important to these processes.

Upon dryout of the bed, the dominant modes of heat transfer are conduction and radiation. There is significant experimental evidence [1, 2] that a fixed packed bed behaves as a continuum. Consequently, one can model the radiation (assuming the bed to be optically thick) through the Rosseland approximation and the conduction by using equivalent thermal conductivity. Owing to the very low conductivity of the dry bed and low efficiency of radiation at relatively low temperatures, melting of steel particles imbedded in the fuel may occur. The melting of the stainless-steel particulate can also be modeled by assuming the bed to be a continuum with conduction and radiation as the dominant mode of heat transfer. The effect of drainage of the molten steel on heat transfer is neglected, and further, it is assumed that it disappears into cracks and mortar joints in the MgO bricks, leaving behind a debris bed of fuel particulate only. The resultant bed readjusts both its height and porosity to accommodate additional space left behind by the drainage of molten steel.

Once again the heat transfer in the bed consisting of fuel particulate alone is modeled as conduction and radiation. Because of lower rates of heat transfer from the bottom of the bed as compared to those from the top, the fuel melting occurs near the lower part of the bed and moves down to the bottom of the bed. The modeling of the fuel melting process in the interior of the bed is identical to that for the steel particulate as described above, except that bed settling during fuel melting is more pronounced than that in the case of steel melting for beds containing a small weight fraction of steel. The bed settling due to gravity and due to the weight of overlying bed and sodium pool is almost instantaneous as compared to the rate of melting of the fuel particulate. Consequently, due to displacement of molten layer, the bed height is continuously adjusted in the modeling. The molten fuel, as it forms a continuous layer over the bottom of the bed, begins to cause the heatup of the MgO lining. When the interface attains the eutectic temperature (2280°C), the MgO lining begins to dissolve in the molten layer of the fuel. The dissolution process lowers the density of the fuel layer (MgO being 2.5 times lighter than pure molten fuel) and causes a density gradient. This density gradient causes destabilization of the molten layer, leading to mixing of dissolved MgO by natural convection. The mixing enhances the disolution process and, consequently, the penetration of the MgO lining. The process of

*Work performed under the auspices of the U.S. Department of Energy.

NOMENCLATURE

A	surface area of debris bed
A_S	total surface area of the solid particles in the bed
a_s	surface area of particles per unit volume of bed
B	total bed loading due to solid particulate [kg m^{-2}]
B_F	bed loading due to fuel particulate [kg m^{-2}]
B_s	bed loading due to steel particulate [kg m^{-2}]
C_p	specific heat at constant pressure
D	particle diameter
g	acceleration due to gravity
h_s	enthalpy of solid stainless steel
h_{sm}	enthalpy of molten steel
K	thermal conductivity
K^*	thermal conductivity of the mixture in the molten pool
k	permeability
k_n	mass transfer coefficient
N	number of solid particles
P	pressure in the debris bed
$\dot{Q}$	heat generation rate per unit volume of bed
q	heat flux
$\dot{q}$	heat generation rate per unit volume of fuel
T	temperature
T_{sm}	melting temperature of steel
T_o	reference temperature
t	time
x, y	local coordinates
Y	position of interfaces in debris bed
Y_F	position void or quench front at the top
u	superficial velocity in x direction
v	superficial velocity in y direction
V	Volume of debris bed.

Greek symbols

β	coefficient of volumetric thermal expansion
γ	defined by equation (6b)
ε	void fraction in the debris bed
ε_F	volume fraction of fuel particulate
ε_s	volume fraction of steel particulate
κ	thermal diffusivity
μ	dynamic viscosity
ν	kinematic viscosity
ξ	defined by equation (5b)
ρ	density
ρ_o	reference density at temperature T_o, concentration C_o
σ	Stefan–Boltzmann constant.

Subscripts

E, e	equivalent
F	fuel
L	lower interface
M	MgO lining
m	UO_2–MgO solution
r	radiation
s	stainless steel
S	solid
SE	solid fuel and steel particulate
T	turbulent
U	upper interface.

penetration of MgO lining continues until the mixing process lowers the concentration of fuel in the volume of pool to a level where internal heat rate per unit volume is not enough to keep the body of the pool molten. Consequently, the freezing process begins in the cooler parts of the molten pool. This freezing process is modeled as two-dimensional as the temperature distribution prior to freezing is governed by mixing in the natural convection mode, which in the present configuration is at least a two-dimensional phenomenon.

If the thickness of the MgO lining is such that it is not being penetrated further because the molten pool has frozen or it reached a quiescent state, then indeed we have determined the 'safe' MgO brick lining thickness for the given bed loading of the fuel and the external rate of cooling.

HEAT TRANSFER IN DRIED-UP DEBRIS BED

If the debris bed is sufficiently deep and decay power level is sufficiently high, sodium coolant subsequent to boiling is likely to leave the bed dry (void of liquid sodium) in spite of the overlying sodium coolant pool. Because of the very high temperatures in the bed, the 'quench front' may not be able to penetrate into the depth of the pool. Upon dryout the debris bed is primarily cooled by conduction and radiation modes of heat transfer. The study of heat transfer characteristics of a dry debris bed are very important as the sequence of processes that follow owing to inadequate cooling of the dry bed could possibly be detrimental to the vessel. If the temperatures continue to rise, the melting of steel in the debris bed and subsequently that of the vessel will occur. Consequently, it is important to determine the temperature distribution of the dry bed as a function of space and time. This calculation also establishes initial conditions for the melting in the debris bed and of the pressure vessel.

Heat transfer model for dried-up bed

Generally, the problem of heat transfer in dry beds at high temperatures is one of interaction between conduction and radiation. Radiation, in one extreme,

for very porous beds consisting of semi-transparent particles can be described by an optically thin approximation. On the other hand, for closely packed opaque particles, radiation can be described by an optically thick approximation. For the treatment of radiation, as for the conduction mode, the dispersed phase is assumed to be a continuum; consequently, the total heat flux in a one-dimensional system can be written as [1]

$$q(y) = q_c(y) + q_r(y) \tag{1}$$

with

$$q_c(x) = -K_E \frac{\partial T}{\partial y} \tag{2}$$

and under optically thick conditions, $q_r(x)$ can be expressed by the Rosseland approximation in terms of a Fourier-type equation as

$$q_r(y) = -K_r \frac{\partial T}{\partial y}. \tag{3}$$

The above representation of the radiation flux implies that radiation transport is considered to be a local effect taking place between surfaces of neighboring particles, and the long-range effects due to the presence of voids are neglected [1]. In view of equations (2) and (3), equation (1) becomes

$$q(y) = -(K_E + K_r)\frac{\partial T}{\partial y} = -K_e \frac{\partial T}{\partial y}. \tag{4}$$

A number of models have been proposed to calculate effective conductivity, K_E, and radiation conductivity, K_r. A very systematic study of these models was performed by Kelly *et al.* [2] to evaluate them experimentally. In-reactor experiments using fission heating of UO_2 particulate to simulate decay heat power levels were conducted and temperatures as high as 3100 K were attained. Both pure UO_2 and mixed UO_2/steel beds were studied. Of the various models investigated, Imura and Takegoshi's [3] model for K_E and Vortmeyer's [1] model for K_r gave good agreement for mixed beds over a wide temperature range. In the present study, these models will be utilized. The Imura–Takegoshi relation [3] for effective thermal conductivity K_E is given as

$$\frac{K_E}{K_g} = \omega + \frac{1-\omega}{\xi + (K_g/K_{SE})(1-\xi)} \tag{5a}$$

where

$$\xi = 0.3\,\varepsilon^{1.6}\left(\frac{K_{SE}}{K_g}\right)^{-0.044} \tag{5b}$$

$$\omega = \frac{\varepsilon - \xi}{1-\xi}. \tag{5c}$$

The equivalent solid conductivity, K_{SE}, for the mixed beds, as suggested by Luikov *et al.* [4], is determined from the Maxwell relation

$$K_{SE} = K_1 \frac{3 - 3\gamma + 2\gamma K_1/K_2}{(3-\gamma)K_1/K_2 + \gamma}, \tag{6a}$$

where

$$\gamma = \frac{\varepsilon_1}{1-\varepsilon}. \tag{6b}$$

Subscript 1 refers to the solids with largest volume fraction and subscript 2 refers to the one with smallest volume fraction.

Vortmeyer's model [1] for radiation thermal conductivity K_r is given as

$$K_r = 4\chi\sigma D T^3 \tag{7}$$

where χ is the radiation exchange factor, which depends on the bed porosity and emissivity of the particles. Kelly *et al.* [2] assumed a value of 0.85 for this parameter for the types of beds of interest to post-accident heat removal.

The equation governing the transient heat transfer as discussed previously must include the effect of radiation and is given as

$$[\varepsilon_F \rho_F C_{PF} + \varepsilon_s \rho_s C_{ps} + \varepsilon \rho_g C_{pg}]\frac{\partial T}{\partial t} = \frac{\partial}{\partial y}\left[(K_E + K_r)\frac{\partial T}{\partial y}\right] + \dot{Q}. \tag{8}$$

The boundary condition that the above equation must satisfy is

$$-(K_E + K_r)\frac{\partial T}{\partial y}\bigg|_{y=0^+} = q|_{y=0^-} \tag{9a}$$

where flux, $q(y = 0^-)$, is calculated by conduction and radiation losses to the lower structure. The boundary condition at the upper end is that of a fixed temperature. However, location of this end needs to be determined by calculations to be carried out in the transient void propagation phase described previously. This location is determined by the position of the quench front. The fixed temperature to be assigned will be equal to the saturation temperature at the pressure corresponding to the location of the quench front. Thus,

$$T|_{y=Y_F(t)} = T_s \tag{9b}$$

where $Y_F(t)$ is the location of the quench front.

STAINLESS-STEEL MELTING AND DRAINAGE

The continuum model of a porous bed is an extremely useful device available to obtain gross or macroscopic behavior of a bed. In analyzing the melting of steel particulate imbedded homogeneously in the fuel debris, the debris bed will be considered to be a continuum. Conduction and radiation are assumed to be the dominant modes of heat transfer. It is further assumed that the volume content of stainless steel is not large enough for drainage of the molten steel to be initiated immediately upon melting. It is held in place by surface tension (during melting) until the temperature of the bed over most of the bed height becomes high enough to lead to the melting of the

majority of the steel. We will also assume: (1) that no significant freezing of the steel occurs as it begins to drain because of higher temperatures prevailing in the lower part of the bed as compared to the upper part; (2) that no significant change in thermal conductivity of the bed occurs due to molten steel as the amount of steel present is not enough to fill the voids in the bed; and (3) that the convection effect due to drainage velocity of the molten steel is negligible as compared to conduction and radiation because of the presence of significant voids in the bed. Consequently, the drainage process and the time necessary to drain will be neglected. Furthermore, as molten steel drains to the bottom of the bed, it escapes into the cracks and mortar joints of the MgO bricks, leaving behind the solid debris bed of fuel. This assumption is valid for debris beds containing amounts of steel equal to or less than the fuel. For debris beds containing large amounts of steel, the molten steel would accumulate at the bottom of the bed after the cracks have been filled.

Governing equations

To date, to the best knowledge of the authors, no previous analytical study of the melting process in a heat-generating debris bed has appeared in the literature. Consequently, the equations governing the melting process need to be formulated. We will start from the following form of the energy equation

$$\frac{\partial}{\partial t}[\varepsilon_F\rho_F C_{PF}(T-T_o)+\varepsilon_s\rho_s h_s+\varepsilon\rho_g C_{pg}(T-T_o)] = \frac{\partial}{\partial y}\left[(K_E+K_r)\frac{\partial T}{\partial y}\right]+\dot{Q} \quad (10)$$

where T_o is a reference temperature. Let $Y_{SL}(t)$ be the position of the lower interface and $Y_{SU}(t)$ be the position of the upper interface. Integrating equation (10) about an interface and using Leibnitz' rule gives

$$\begin{aligned}\frac{\partial}{\partial t}\int_{Y_S^-}^{Y_S^+}&[\varepsilon_F\rho_F C_{PF}(T-T_o)+\varepsilon_s\rho_s h_s\\&+\varepsilon\rho_g C_{pg}(T-T_o)]\,dy\\&-[\varepsilon_F\rho_F C_{PF}(T-T_o)+\varepsilon_s\rho_s h_s\\&+\varepsilon\rho_g C_{pg}(T-T_o)]|_{Y=Y_S^+}\dot{Y}_S^+\\&+[\varepsilon_F\rho_F C_{PF}(T-T_o)+\varepsilon_s\rho_s h_s\\&+\varepsilon\rho_g C_{pg}(T-T_o)]|_{y=Y_S^-}\dot{Y}_S^-\\&=(K_E+K_r)\frac{\partial T}{\partial y}\bigg|_{Y_S^+}-(K_E+K_r)\frac{\partial T}{\partial y}\bigg|_{Y_S^-}+\int_{Y_S^-}^{Y_S^+}\dot{Q}\,dy.\end{aligned} \quad (11)$$

Taking the limit of Y_S^- and Y_S^+ approaching Y_S and assuming the temperature is continuous across the interface, we obtain the following interface balance equation for the lower interface

$$-\varepsilon_s\rho_s\Delta h_s\dot{Y}_{SL}=(K_E+K_r)\frac{\partial T}{\partial y}\bigg|_{Y_{SL}^+}-(K_E+K_r)\frac{\partial T}{\partial y}\bigg|_{Y_{SL}^-} \quad (12a)$$

where $\Delta h_s = h_{sm}-h_s$, h_{sm} is the enthalpy of molten steel. For the upper interface we have

$$\varepsilon_s\rho_s\Delta h_s\dot{Y}_{SU}=(K_E+K_r)\frac{\partial T}{\partial y}\bigg|_{Y_{SU}^+}-(K_E+K_r)\frac{\partial T}{\partial y}\bigg|_{Y_{SU}^-}. \quad (12b)$$

Energy equation (10) applies both to the molten region and to the solid region. The boundary conditions that it must satisfy are:

—at the upper and lower liquid interfaces

$$T|_{Y_S}=T_{sm} \quad (13)$$

—at the debris bottom

$$-(K_E+K_r)\frac{\partial T}{\partial y}=q|_{0-}. \quad (14)$$

At the upper part of the debris, a fixed temperature boundary condition equal to the saturation temperature of sodium vapor is used. Thus,

$$T|_{Y_F}=T_{sat}, \quad (15)$$

where the Y_F is the position of the 'quench front' obtained from analysis described in ref. [5].

MELTING OF FUEL DEBRIS AND FORMATION OF MOLTEN POOL

Following melting of the steel particulate and its subsequent drainage to the bottom of the bed, the molten steel layer may disappear into mortar cracks leaving behind a dry debris bed consisting of fuel particulate only (valid for small amounts of steel). Once again, the prevalent modes of heat transfer are conduction and radiation. It is anticipated that heat loss from the debris bed will be higher to the overlying sodium pool as compared with MgO substrate. Consequently, maximum temperature will occur somewhere in the lower part of the bed. If the heating of the bed continues with imbalance in heat losses from it, fuel debris will melt at its maximum temperature. Subsequently, the melting will spread into the rest of the bed with the lower part melting first.

With the melting of the lower or the bottom part of the particulate, the bed settles and becomes partially submerged in the molten layer. The height of the molten layer increases as it begins to dissolve the MgO lining at the bottom and as more molten fuel adds to it, due to particulate melting. The dissolution of the MgO in the molten layer of fuel will tend to decrease the density of solution near the bottom and lead to mixing by natural convection.

Assumptions

1. Heat transfer in dry debris bed prior to and during fuel melting is dominantly governed by conduction and radiation modes.

2. The debris bed behaves like a continuum both for conduction and radiation modes of heat transfer and for treating melting.

3. The bed continuously settles at a rate equal to the rate of melting.

4. The rate at which molten fuel is increasing in the molten pool forming at the bottom of the bed is equal to the rate at which fuel is melting; that is, we assume no freezing of the molten fuel as it drains.

5. The dissolution of the MgO lining in the molten UO_2 will also contribute to the increase in the height of the pool as the density of molten MgO (2400 vs 3400 kg m^{-3} for solid phase) is significantly less than the density of the solid phase.

6. The convection currents due to density gradients caused by the dissolution of MgO will dominate the mixing process in the pool.

7. The effect of the presence of MgO in the molten pool on lowering the melting temperature for fuel particulate will be taken into account through the phase diagram given in Fig. 1 (the data points shown in this figure are taken from ref. [8]).

The fourth assumption is a reasonably valid assumption in view of the fact that the maximum temperatures occur in the bottom part of the debris bed and, therefore, melting in the lower part will be simultaneous. This assumption becomes even more valid as the bed begins to get immersed more and more in the molten layer of the fuel. Furthermore, we will neglect the time taken by molten fuel to drain and assume that it joins the molten pool instantly. This assumption becomes more valid as the height of the molten pool increases and the bed becomes more and more immersed in the pool.

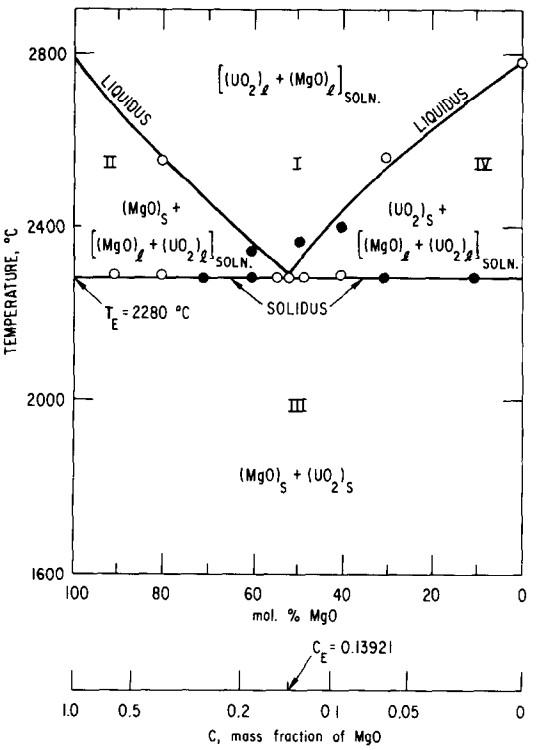

FIG. 1. Phase diagram for MgO–UO_2 system.

Heatup of dry fuel bed

During the heatup of the dry bed, the dominant modes of heat transfer are conduction and radiation. The governing equations have been described previously; however, we give these equations below when particulate material consists of fuel only, that is, $\varepsilon_F = 1-\varepsilon$,

$$[(1-\varepsilon)\rho_F C_{PF} + \varepsilon\rho_g C_{pg}]\frac{\partial T}{\partial t} = \frac{\partial}{\partial y}\left[(K_{FE}+K_r)\frac{\partial T}{\partial y}\right]+\dot{Q}, \quad (16)$$

where ε is now given by [6]

$$\varepsilon = 0.593-1.23\times 10^{-4}B_F, \quad (17)$$

with the debris bed height given by

$$H_{F0} = \frac{B_F}{(1-\varepsilon)\rho_F}. \quad (18)$$

The equivalent thermal conductivity, K_{FE}, of the dry debris bed is given by Imura and Takegoshi's empirical expression [3]

$$\frac{K_{FE}}{K_g} = \omega + \frac{1-\omega}{\xi+(K_g/K_F)(1-\xi)}, \quad (19a)$$

where

$$\xi = 0.3\,\varepsilon^{1.6}\left(\frac{K_F}{K_g}\right)^{-0.044} \quad (19b)$$

$$\omega = \frac{\varepsilon-\xi}{1-\xi}. \quad (19c)$$

The equivalent thermal conductivity, K_r, for radiation is given by Vortmeyer's model [1], cf. equation (7). The discussion of the boundary conditions for equation (16) is given previously. These conditions are given by equations (9a) and (9b).

Initial melting of the fuel debris bed and formation of the molten layer

The peak temperatures in the dry fuel debris bed, as discussed previously, occur in the lower part of the bed near the bottom. Consequently, melting will occur first in this part and spread downwards. The melting of the debris will lead to settling of the bed because of the removal of the void volume. The melting process is a much slower process as compared with bed settling (by 'free' fall) and, consequently, it is reasonable to assume that the latter process occurs instantly due to the weight of the overlying debris bed. It then follows that the height of the bed at any time is equal to the sum of heights of the unmolten portions of the bed. This statement is true until all available void volume is filled with molten material.

As it collects at the bottom, the molten fuel does not spread out to cover the surface of the substrate until it achieves a critical thickness H_c given by [7]

$$H_c = (\sigma_F/\rho g)^{1/2}. \quad (20)$$

The above relation is an order of magnitude estimate of thickness of the molten layer, below which it will not spread. The above equation is obtained by requiring a balance between surface tension and gravity forces. Here, σ_F is the surface tension of molten fuel and ρ_{FM} is the density of molten fuel. Consequently, if molten fuel in the porous bed does not accumulate to height H_c, it will be incapable of covering the substrate surface in the form of a liquid film and, as a result, dissolution will be negligible. After molten fuel accumulates to this height, we will include the effect of dissolution of MgO, both in the formation of the pool through the addition of mass and its effect on the rate of melting of the fuel particulates submerged in this growing molten layer.

The equations governing the positions of the lower and upper melt interfaces are readily obtained by adapting equation (12) to fuel particulate as

$$(1-\varepsilon)\rho_F\Delta h_F\dot{Y}_{FL} = (K_{FE}+K_r)\frac{\partial T}{\partial y}\bigg|_{Y_{FL}^+} - (K_{FE}+K_r)\frac{\partial T}{\partial y}\bigg|_{Y_{FL}^-} \quad (21)$$

$$(1-\varepsilon)\rho_F\Delta h_F\dot{Y}_{FU} = (K_{FE}+K_r)\frac{\partial T}{\partial y}\bigg|_{Y_{FU}^+} - (K_{FE}+K_r)\frac{\partial T}{\partial y}\bigg|_{Y_{FU}^-}. \quad (22)$$

The above equations, however, need to be modified to account for bed settling as a result of melting. Since bed settling is assumed to be instantaneous, that is, molten fuel is forced down or removed due to the weight of the overlying unmolten bed until, of course, the whole of the bottom part becomes molten, at which time melting begins to proceed from the bottom up. In view of this discussion, equation (21) simplifies to

$$(1-\varepsilon)\rho_F\Delta h_F\dot{Y}_{FL} = (K_{FE}+K_r)\frac{\partial T}{\partial y}\bigg|_{Y_{FL}^-}. \quad (23)$$

In order to include the effect of bed settling in modeling the upper interface, we first shift the coordinate origin from the bottom to the top of the bed. Let H_{FO} be the height prior to the inception of melting (see Fig. 2a). Thus,

$$y' = H_{FO} - y. \quad (24)$$

Using the above transformation in equation (22) and accounting for bed settling, we have

$$(1-\varepsilon)\rho_F\Delta h_F\dot{Y}' = (K_{FE}+K_r)\frac{\partial T}{\partial y'}\bigg|_{Y'^-}. \quad (25)$$

The height, $H_F(t)$, of the bed while it is continuously settling is given as (see Fig. 2b)

$$H_F(t) = Y_{FL} + |Y'|, \quad (26)$$

and the height $Y_P(t)$ of the molten layer collecting at the bottom is obtained from mass conservation as (see Fig. 2)

$$\rho_{FM}\varepsilon Y_P(t) = [H_{FO} - H_F](1-\varepsilon)\rho_F. \quad (27)$$

The expression is valid as long as $Y_P \leqslant H_c$. This equation will not be an accurate representation if voids are only partially filled. This indeed will be the case if Y_P is less than the size of the particles.

Dissolution of the MgO lining and fuel particulate

The molten layer, as it accumulates over the bottom of the bed, begins to cause heatup of the MgO lining. The particulate submerged in the molten layer, because of its small size, very quickly attains thermal equilibrium with the molten layer. When the interface attains the eutectic temperature (2280°C), the MgO lining begins to dissolve in the molten layer of the fuel. The dissolution process lowers the density of the fuel layer (MgO being 2.5 times lighter than pure molten fuel) and causes a density gradient. This density gradient causes destabilization of the molten layer leading to mixing of dissolved MgO by natural convection. The mixing enhances the dissolution process and, consequently, the penetration of the MgO lining. The addition of MgO components in the molten layer causes dilution of the heat generating component, namely, fuel. This dilution begins to lower the melting

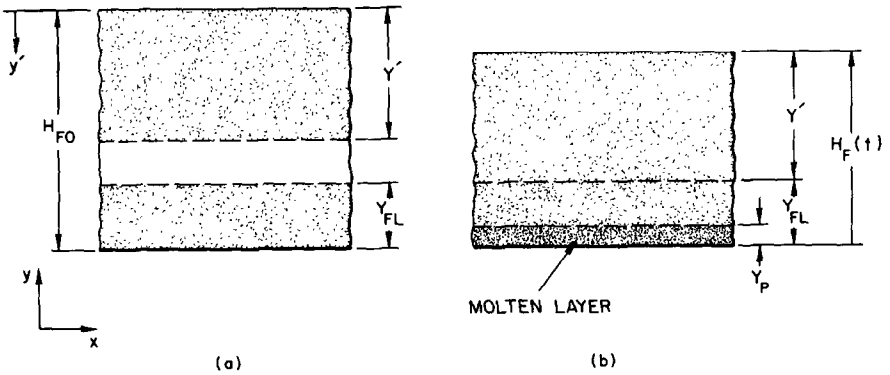

FIG. 2. Position of molten interfaces during the melting of fuel particulate (a) without bed settling and (b) with bed settling.

temperature of fuel particulate immersed in the molten layer and cause their dissolution.

The melting of fuel particulate in the volume of the dried-out bed and the dissolution of MgO lining and of the fuel particulate immersed in the molten layer all contribute to increasing the height Y_P of the molten layer. The mass balance for this molten layer gives (see Fig. 3):

$$\int_0^{Y_P} \rho\varepsilon \, dy_o = \rho_M Y_b + (H_{FO} - H_F)(1-\varepsilon)\rho_F + \rho_F \int_0^{Y_P} \left[1 - \left(\frac{R}{R_o}\right)^3\right] dy_o. \quad (28)$$

The term on the LHS gives the total mass contained in the molten layer, the first term on the RHS gives the mass of MgO lining that dissolved, the second term represents the mass of molten particulate in the dried up bed. The third term gives the mass of particulate that dissolved in the molten layer. All of these masses are expressed per unit area of the bed. The derivation of the last term on the LHS is given in Appendix A.

The equations governing heat and mass transfer in the molten layer and those describing dissolution of the particulate and MgO lining are given as:

Molten layer and submerged particulate

$$\frac{\partial[\varepsilon\rho + (1-\varepsilon)\rho_F]}{\partial t} + \frac{\partial}{\partial x}(\rho u) + \frac{\partial}{\partial y}(\rho v) = 0 \quad (29)$$

$$\frac{\partial \varepsilon\rho C}{\partial t} + \frac{\partial \rho u C}{\partial x} + \frac{\partial \rho v C}{\partial y} = \frac{\partial}{\partial x}\left(\rho D \frac{\partial C}{\partial x}\right) + \frac{\partial}{\partial y}\left(\rho D \frac{\partial C}{\partial y}\right) - k_N a_s \rho [C - C_s(T_m)] \quad (30)$$

$$\frac{\partial}{\partial t}\{(1-\varepsilon)\rho_F C_{PF}(T_m - T_R) + [1-(R/R_o)^3] \times \rho_F \Delta h_F + \varepsilon\rho h\} + \frac{\partial(\rho u h)}{\partial x} + \frac{\partial}{\partial y}(\rho v h) = \frac{\partial}{\partial x}\left(K^* \frac{\partial T}{\partial x}\right) + \frac{\partial}{\partial y}\left(K^* \frac{\partial T}{\partial y}\right) + \dot{q} \quad (31)$$

$$\frac{\partial}{\partial t}\{\rho_F A[1-(R/R_o)^3]\, dy_o\} = k_N A_s \rho [C_s(T) - C],$$

or

$$\frac{\partial}{\partial t}\{\rho_F[1-(R/R_o)^3]\} = \frac{3(1-\varepsilon)}{R} k_N \rho (C_s - C) = a_s k_N (C_s - C) \quad (32)$$

$$u = -\frac{k_m}{\mu_m}\frac{\partial P}{\partial x} \quad (33)$$

$$v = \frac{k_m}{\mu_m}\left(-\frac{\partial P}{\partial y} + \rho g\right) \quad (34)$$

$$\rho = \rho_E + \left(\frac{\partial \rho}{\partial T}\right)_P (T - T_E) + \left(\frac{\partial P}{\partial C}\right)_P (C - C_E), \quad (35a)$$

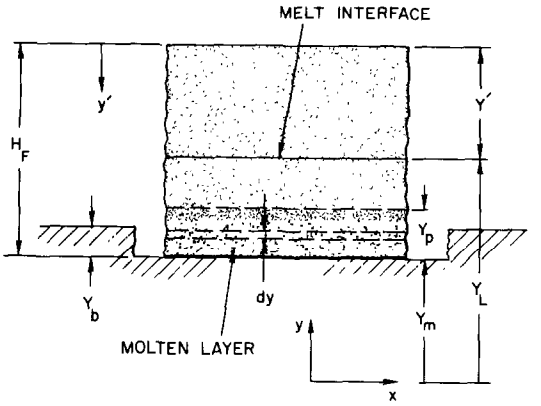

FIG. 3. Simultaneous dissolution of MgO substrate and fuel particulate submerged in molten solution of UO_2 and MgO.

where the reference state is taken at eutectic composition of UO_2–MgO solution. The density at reference state is computed as

$$\rho_E = C_E \rho_{MgO} + (1 - C_E)\rho_{UO_2}. \quad (35b)$$

In equation (31), the term $[1-(R/R_o)^3]\ \rho_F \Delta h_F$ represents heat of dissolution; its derivation is given in equation (A5) of Appendix A.

The interface balance equations governing the dissolution of MgO lining are given in Appendix B. These equations are given below:

$$v_m = \frac{1}{\rho_E}(\varepsilon\rho_E + (1-\varepsilon)\rho_F - \rho_{MgO_S})\dot{Y}_m \quad (36)$$

$$\{\rho_{MgO_S} - [1-(R/R_o)^3]\}(1-C_E)\dot{Y}_m = \rho_E D \left.\frac{\partial C}{\partial y}\right|_{Y_m} \quad (37)$$

$$\{\rho_{MgO_S}(h_{MgO_S} - h_E) + (1-\varepsilon)\rho_F[h_E - C_{PF}(T_m - T_R)] - \rho_F[1-(R/R_o)^3]\Delta h_F\}\dot{Y}_m = K^* \left.\frac{\partial T}{\partial y}\right|_{Y_m^+} - K_{MgO_S} \left.\frac{\partial T}{\partial y}\right|_{Y_m^-}. \quad (38)$$

MOLTEN POOL PENETRATION AND FREEZING

Following the complete melting and dissolution of fuel particles of debris bed, a molten pool consisting of solution of UO_2 and MgO is formed. The molten pool thus formed continues to penetrate the MgO lining by dissolving it. The equations governing the dissolution of MgO lining and its subsequent mixing by turbulent natural convection are given as:

Conservation of mass

$$\frac{\partial u}{\partial x} + \frac{\partial v}{\partial y} = 0. \quad (39)$$

Conservation of momentum

$$\frac{\partial u}{\partial t}+u\frac{\partial u}{\partial x}+v\frac{\partial u}{\partial y}$$
$$=-\frac{1}{\rho_o}\frac{\partial P}{\partial x}+\frac{1}{\rho_o}\frac{\partial}{\partial x}\left(\mu\frac{\partial u}{\partial x}\right)+\frac{1}{\rho_o}\frac{\partial}{\partial y}\left(\mu\frac{\partial u}{\partial y}\right)$$
$$+\frac{\partial}{\partial y}\left(\nu_T\frac{\partial u}{\partial y}\right)+\frac{\partial}{\partial y}\left(\nu_T\frac{\partial v}{\partial x}\right) \quad (40)$$

$$\frac{\partial v}{\partial t}+u\frac{\partial v}{\partial x}+v\frac{\partial v}{\partial y}$$
$$=-\frac{1}{\rho_o}\frac{\partial P}{\partial y}+g[\beta(T-T_o)+\beta_c(C-C_o)]$$
$$+\frac{1}{\rho_o}\frac{\partial}{\partial x}\left(\mu\frac{\partial v}{\partial x}\right)+\frac{1}{\rho_o}\frac{\partial}{\partial y}\left(\mu\frac{\partial v}{\partial y}\right)$$
$$+\frac{\partial}{\partial x}\left(\nu_T\frac{\partial u}{\partial x}\right)+\frac{\partial}{\partial y}\left(\nu_T\frac{\partial v}{\partial y}\right). \quad (41)$$

Conservation of energy

$$\frac{\partial T}{\partial t}+u\frac{\partial T}{\partial x}+v\frac{\partial T}{\partial y}$$
$$=\frac{\partial}{\partial x}\left[\left(\alpha+\frac{\nu_T}{\sigma_T}\right)\frac{\partial T}{\partial x}\right]+\frac{\partial}{\partial y}\left[\left(\alpha+\frac{\nu_T}{\sigma_T}\right)\frac{\partial T}{\partial y}\right]$$
$$+\frac{\partial}{\partial y}\left(\frac{\nu_T}{\sigma_T}\frac{\partial T}{\partial y}\right)+\frac{\dot{q}}{\rho_o C_p}. \quad (42)$$

Conservation of species

$$\frac{\partial C}{\partial t}+u\frac{\partial C}{\partial x}+v\frac{\partial C}{\partial y}$$
$$=\frac{\partial}{\partial x}\left[\left(D+\frac{\nu_T}{\sigma_c}\right)\frac{\partial C}{\partial x}\right]+\frac{\partial}{\partial y}\left[\left(D+\frac{\nu_T}{\sigma_c}\right)\frac{\partial C}{\partial y}\right]. \quad (43)$$

Interface balance for dissolution or freezing

Integrating mass continuity equation for the solution over the strip lying across the interface as shown in Fig. 4, we obtain

$$\int\int\frac{\partial\rho}{\partial t}\,dx\,dy+\int\int\left(\frac{\partial\rho u}{\partial x}+\frac{\partial\rho v}{\partial y}\right)dx\,dy=0 \quad (44)$$

or

$$\int_x^{x+dx}\int_{a(x,t)}^{b(x,t)}\frac{\partial\rho}{\partial t}\,dy\,dx+\int_x^{x+dx}\int_{a(x,t)}^{b(x,t)}\times\frac{\partial\rho u}{\partial x}\,dy\,dx+\int_x^{x+dx}\int_{a(x,t)}^{b(x,t)}\frac{\partial\rho v}{\partial y}\,dy\,dx=0. \quad (45)$$

Applying Leibnitz' rule

$$\int_x^{x+dx}\left[\frac{\partial}{\partial t}\int_a^b\rho\,dy-\rho_b\frac{\partial b}{\partial t}+\rho_a\frac{\partial a}{\partial t}\right]dx+\int_x^{x+dx}\times\left[\frac{\partial}{\partial x}\int_a^b\rho u\,dy-(\rho u)_b\frac{\partial b}{\partial x}+(\rho u)_a\frac{\partial a}{\partial x}\right]dx+\int_x^{x+dx}[(\rho v)_b-(\rho v)_a]\,dx=0. \quad (46)$$

Noting that on the side of solid $u=v=0$ and letting $a\to b\to Y_m$, we obtain for melting and freezing

$$\frac{\rho_m-\rho_{sm}}{\rho_m}\frac{\partial Y_m}{\partial t}=v_m-u_m\frac{\partial Y_m}{\partial x}. \quad (47)$$

Here, ρ_m = density of solution at interface, ρ_{sm} = density of solid at interface, u_m, v_m = x, y components of velocities at the interface.

Similarly, the integration of energy equations across the interface gives

$$\int\int\frac{\partial\rho H}{\partial t}\,dx\,dy+\int\int\frac{\partial\rho uH}{\partial x}\,dx\,dy+\int\int\frac{\partial\rho vH}{\partial y}\,dx\,dy=-\int\int\frac{\partial q_x}{\partial x}\,dx\,dy-\int\int\frac{\partial q_y}{\partial x}\,dx\,dy+\int\int\dot{q}\,dx\,dy. \quad (48)$$

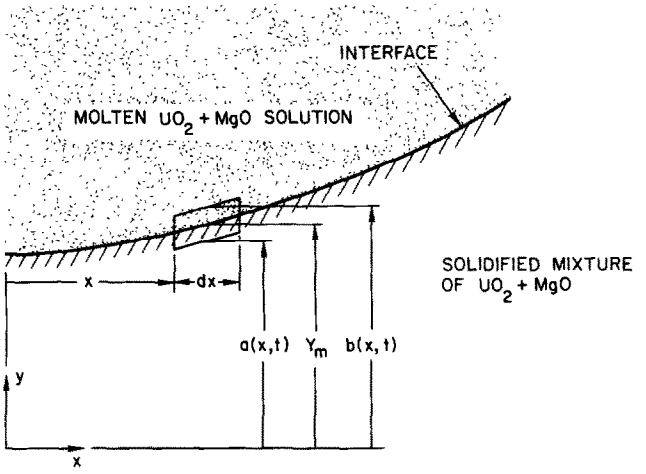

FIG. 4. Control volume across interface between molten solution of UO_2 and MgO and solidified mixture of UO_2 and MgO or MgO substrate.

Both for melting and freezing, the above equation becomes

$$\rho_m \Delta h \frac{\partial Y_m}{\partial t} = K_{sm}\left(\frac{\partial T}{\partial y}\right)_{Y_m^-} - K_m\left(\frac{\partial T}{\partial y}\right)_{Y_m^+} - \left[K_{sm}\left(\frac{\partial T}{\partial x}\right)_{Y_m^+} - K_m\left(\frac{\partial T}{\partial x}\right)_{Y_m^+}\right]\frac{\partial Y_m}{\partial x}. \quad (49)$$

The integration of concentration balance equation across the interface gives

$$\int\int \frac{\partial \rho C}{\partial t}\,dx\,dy + \int\int \frac{\partial}{\partial x}(\rho u C)\,dx\,dy + \int\int \frac{\partial}{\partial y}(\rho v C)\,dx\,dy = -\int\int \frac{\partial j_x}{\partial x}\,dx\,dy - \int\int \frac{\partial j_y}{\partial y}\,dx\,dy \quad (50)$$

where $j_x, j_y = x, y$ components of diffusional fluxes.

Both for melting and freezing, the above equation simplifies to

$$\rho_{sm}(C_{sm} - C_m)\frac{\partial Y_m}{\partial t} + \rho_m\left(D\frac{\partial C}{\partial x}\right)_{Y_m^+}\frac{\partial Y_m}{\partial x} - \rho_m\left(D\frac{\partial C}{\partial y}\right)_{Y_m^+} = 0, \quad (51)$$

where C_{sm} is the concentration of MgO in the solid phase, C_M is the concentration of MgO in the solution.

CONCLUDING REMARKS

The process of penetration of MgO lining continues until the mixing process lowers the concentration of fuel in the volume of the pool to a level where internal heat rate per unit volume is not enough to keep the body of the pool molten. Consequently, the freezing process begins in the cooler parts of the molten pool. This freezing process is modeled as two-dimensional as the temperature distribution prior to freezing is governed by mixing in the natural convection mode which in the present configuration is at least a two-dimensional phenomenon.

If the thickness of the MgO lining is such that it is not being penetrated further because the molten pool has frozen or it reached a quiescent state, then indeed we have determined the 'safe' MgO brick lining thickness for the given bed loading of the fuel and the external rate of cooling.

REFERENCES

1. D. Vortmeyer, Radiation in packed solids, *Sixth International Heat Transfer Conference*, Toronto, Canada, Vol. 6, p. 525 (1978).
2. J. E. Kelly, M. L. Schwarz and J. T. Hitchcock, Heat transfer characteristics of dry porous particulate beds with internal heat generation, *Proc of ASME/JSME Thermal Engineering Joint Conference*, Honolulu, Hawaii, Vol. 4, p. 83 (1983).
3. S. Imura and E. Takegoshi, Effect of gas pressure on the effective thermal conductivity of packed beds, *Heat Transfer—Jap. Res.* **3**, 13 (1974).
4. A. V. Luikov, A. G. Shashkov, L. L. Vasiliev and Yu. E. Fraiman, Thermal conductivity of porous systems, *Int. J. Heat Mass Transfer* **11**, 117 (1968).
5. T. C. Chawla, D. R. Pedersen and W. J. Minkowycz, Governing equations for heat and mass transfer in heat generating porous beds—I. Coolant boiling and transient void propagation, *Int. J. Heat and Mass Transfer* **28**, Ms 169 (1985).
6. J. D. Gabor, E. S. Sowa, L. Baker, Jr, and J. C. Cassulo, Studies and experiments on heat removal from fuel debris in sodium, CONF-740401-P2, *Proc. ANS Fast Reactor Safety Meeting*, Beverly Hills, p. 823 (1974).
7. J. A. Fay, The spread of oil slicks on a calm sea. In *Oil on the Sea* (Edited by D. P. Hoult). Plenum Press, New York (1969).
8. P. O. Budnikov, S. G. Tresvyatsky and V. I. Kishakovsky, Binary phase diagrams for UO_2–Al_2O, UO_2–BeO and UO_2–MgO, *Proc. U.N. Int. Conference Peaceful Uses of Atomic Energy*, Geneva, Vol. 6, pp. 130 (1958).

APPENDIX A: DISSOLUTION OF FUEL PARTICULATE

Due to dissolution of MgO lining in the molten layer of fuel at the bottom of the bed and its subsequent mixing due to natural convection, the concentration of MgO in the layer steadily increases. This increase in concentration of MgO in the solution lowers the melting point of the submerged fuel particulate and, consequently, the particulate begins to dissolve in the solution. As the dissolution proceeds the bed settles, due to its own weight and due to the weight of the overlying pool. However, due to very slow rate of the dissolution, bed settling or movement due to this process alone is very slow compared with that due to melting of fuel particulate in the volume of the bed and that due to dissolution of the MgO lining. Because of its very slow rate of settling, one can assume that the space vacated by dissolution is taken up by settling of the particles from above, so that the void distribution throughout the bed remains invariant at its original value ε.

Let N be the number of particles contained in elemental height δy_{oi} at height y_o prior to inception of dissolution, and let after passage of time t from inception of dissolution, the same number of particles be contained in elemental height δy_i at height y. Since porosity remains invariant, then one writes

$$N = \frac{A(1-\varepsilon)\delta y_{oi}}{\frac{4}{3}\pi R_o^3} = \frac{A(1-\varepsilon)\delta y_i}{\frac{4}{3}\pi R^3}, \quad (A1)$$

where R_o and R is the radii of the particles prior to and during the dissolution process. The above equation yields

$$\delta y_{pi} = \delta y_{oi} - \delta y_i = [1-(R/R_o)^3]\delta y_{oi}. \quad (A2)$$

Clearly, δy_{pi} represents an elemental settling or displacement of the bed over original elemental height δy_{oi}. If Y_p is the height of the molten pool and ΔY_p the total height through which it settles or the total distance through which the bed sinks, then one obtains from equation (A2)

$$\Delta Y_p = \sum_i \delta y_{pi} = \sum_i \frac{R_o^3 - R^3}{R_o^3}\delta y_{oi}$$

or (A3)

$$\Delta Y_p = \int_o^{Y_P} [1-(R/R_o)^3]\,dy_o.$$

If m_D is the total amount of liquid fuel at time t due to

dissolution of particulates in height Y_p, one then obtains from equation (A3)

$$m_D = \rho_F \Delta Y_p A = \rho_F A \int_0^{Y_p} [1-(R/R_o)^3]\,dy_o. \quad (A4)$$

The heat of dissolution absorbed per unit volume is obtained from equation (A2) as

$$\Delta h_D = \rho_F[1-(R/R_o)^3]\Delta h_F, \quad (A5)$$

where Δh_F is the latent heat of fusion for the fuel.

APPENDIX B: INTERFACE BALANCES BETWEEN MOLTEN LAYER AND MgO LINING

We will assume that penetration of the MgO lining is one-dimensional, that is, we will ignore the edge effects as the lateral extent of the bed is sufficiently large. Also, at the same time, we will assume that heat transfer in the MgO lining is governed by one-dimensional conduction equation.

Mass balance

Integrating mass continuity equation for mixture of UO_2–MgO solution and fuel particulate on one side and MgO lining on the other side of the interface (see Fig. B1), we obtain

$$\int\int \frac{\partial[\varepsilon\rho+(1-\varepsilon)\rho_F]}{\partial t}\,dx\,dy + \int\int\left(\frac{\partial \rho u}{\partial x}+\frac{\partial \rho v}{\partial y}\right)dx\,dy = 0 \quad (B1)$$

or

$$\int_x^{x+dx}\int_{a(x,t)}^{b(x,t)} \frac{\partial[\rho\varepsilon+(1-\varepsilon)\rho_F]}{\partial t}\,dy\,dx + \int_x^{x+dx}\int_{a(x,t)}^{b(x,t)} \times \frac{\partial \rho u}{\partial x}\,dy\,dx + \int_x^{x+dx}\int_{a(x,t)}^{b(x,t)} \frac{\partial \rho v}{\partial y}\,dy\,dx = 0. \quad (B2)$$

Applying Leibnitz' rule

$$\int_x^{x+dx}\left\{\frac{\partial}{\partial t}\int_a^b [\varepsilon\rho+(1-\varepsilon)\rho_F]-[\varepsilon\rho_b+(1-\varepsilon)\rho_F]\frac{\partial b}{\partial t} + \rho_a\frac{\partial a}{\partial t}\right\}dx + \int_x^{x+dx}\left[\frac{\partial}{\partial x}\int_a^b \rho u\,dy-\rho_b u_b\frac{\partial b}{\partial x} + \rho_a u_a\frac{\partial a}{\partial x}\right]dx + \int_x^{x+dx}(\rho_b v_b-\rho_a v_a)\,dx = 0. \quad (B3)$$

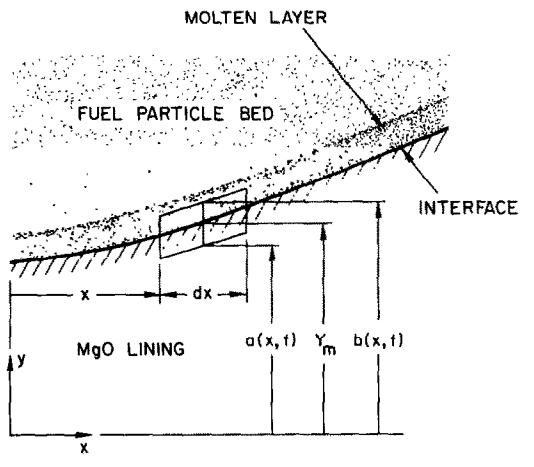

FIG. B1. Control volume across the interface between molten layer of UO_2 and MgO solution and MgO lining in the fuel particulate bed.

where subscripts a and b denote the quantities corresponding to positions a and b, respectively, across the interface. Noting that on the side of MgO lining $u = v = 0$. On letting $a \to b \to Y_m$ (where Y_m denotes the position of the interface from some fixed location), we obtain

$$\frac{\rho_{MgO_S}-[\varepsilon\rho_E+(1-\varepsilon)\rho_F]}{\rho_E}\frac{\partial Y_m}{\partial t} = u_m\frac{\partial Y_m}{\partial x} - V_m, \quad (B4)$$

where ρ_E is the density of the solution at eutectic composition and ρ_{MgO_S} is the density of solid MgO.

Assuming penetration to be one-dimensional, the above equation simplifies to

$$V_m = \frac{\varepsilon\rho_E+(1-\varepsilon)\rho_F-\rho_{MgO_S}}{\rho_E}\frac{dY_m}{dt}. \quad (B5)$$

Concentration balance

Integrating the combination of equations (31) and (32) for UO_2–MgO solution and fuel particulate on one side and solid MgO on the other side of the interface, we obtain

$$\int\int\frac{\partial}{\partial t}\{\varepsilon\rho C+[1-(R/R_o)^3]\rho_F\}\,dx\,dy + \int\int\frac{\partial \rho u C}{\partial x}\,dx\,dy + \int\int\frac{\partial \rho v C}{\partial y}\,dx\,dy = \int\int\frac{\partial}{\partial x}\left(\rho D\frac{\partial C}{\partial x}\right)dx\,dy + \int\int\frac{\partial}{\partial y}\left(\rho D\frac{\partial C}{\partial y}\right)dx\,dy. \quad (B6)$$

As before, upon applying the Leibnitz theorem, we obtain

$$\begin{aligned}&\int_x^{x+dx}\left\{\frac{\partial}{\partial t}\int_{a(x,t)}^{b(x,t)}(\varepsilon\rho C+[1-(R/R_o)^3]\rho_F)\,dx\,dy - \{\varepsilon\rho_b C_b+[1-(R/R_o)^3]\}\frac{\partial b}{\partial t}+\rho_{MgO_S}\frac{\partial a}{\partial t}\right\}dx \\ &+\int_x^{x+dx}\left[\frac{\partial}{\partial x}\int_a^b \rho u C\,dy-\rho_b u_b C_b\frac{\partial b}{\partial x}+\rho_a u_a C_a\frac{\partial a}{\partial x}\right]dx \\ &+\int_x^{x+dx}(\rho_b v_b C_b-\rho_a v_a C_a)\,dx \\ &=\int_x^{x+dx}\left[\frac{\partial}{\partial x}\int_{a(x,t)}^{b(x,t)}\rho D\frac{\partial C}{\partial x}\,dy-\rho_b D\frac{\partial C}{\partial x}\Big|_b\frac{\partial b}{\partial x} + \rho_a D_a\frac{\partial C}{\partial x}\Big|_a\frac{\partial a}{\partial x}\right]dx \\ &+\int_x^{x+dx}\left[\rho_b D\frac{\partial C}{\partial y}\Big|_b-\rho_a D_a\frac{\partial C}{\partial y}\Big|_a\right]dx. \end{aligned} \quad (B7)$$

Letting $a \to b \to Y_m$ and noting that $u_a = v_a = D_a = 0, C_a = 1$, we obtain

$$\{\rho_{MgO_S}-(\varepsilon\rho_E C_E+[1-(R/R_o)^3]\rho_F)\}\frac{\partial Y_m}{\partial t}-\rho_E u_m C_E\frac{\partial Y_m}{\partial x} + \rho_E v_m C_E = -\rho_E D\frac{\partial C}{\partial x}\Big|_{Y_m}\frac{\partial Y_m}{\partial x}+\rho_E D\frac{\partial C}{\partial y}\Big|_{Y_m}. \quad (B8)$$

Substituting for v_m from equation (B4), we obtain

$$\{\rho_{MgO_S}-[1-(R/R_o)^3]\rho_F\}(1-C_E)\frac{\partial Y_m}{\partial t} = -\rho_E D\frac{\partial C}{\partial x}\Big|_{Y_m}\frac{\partial Y_m}{\partial x}+\rho_E D\frac{\partial C}{\partial y}\Big|_{Y_m}, \quad (B9)$$

which for one-dimensional penetration of MgO substrate becomes

$$\{\rho_{MgO_S}-[1-(R/R_o)^3]\rho_F\}(1-C_E)\dot{Y}_m=\rho_E D\frac{\partial C}{\partial y}\bigg|_{Y_m}. \quad \text{(B10)}$$

Heat balance

Integrating equation (31) for UO_2–MgO solution and fuel particulate on one side and MgO lining on the other side of the interface, we obtain

$$-\{(1-\varepsilon)\rho_F C_{PF}(T_m-T_R)+[1-(R/R_o)^3]\rho_F\Delta h_F+\varepsilon\rho h\}_b\frac{\partial b}{\partial t}$$
$$+(\rho h)_a\frac{\partial a}{\partial t}-(\rho uh)_b\frac{\partial b}{\partial x}+(\rho hv)_b$$
$$=-\left(K^*\frac{\partial T}{\partial z}\right)_b\frac{\partial b}{\partial x}+\left(K\frac{\partial T}{\partial x}\right)_a\frac{\partial a}{\partial x}+\left(K^*\frac{\partial T}{\partial y}\right)_b-\left(K\frac{\partial T}{\partial y}\right)_a. \quad \text{(B11)}$$

Letting $a\to b\to Y_m$ and then substituting for v_m from equation (B4), we obtain

$$[\rho_{MgO_S}h_{MgO_S}-\rho_{MgO_S}h_E+\varepsilon\rho_E h_E+(1-\varepsilon)\rho_F h_E$$
$$-(1-\varepsilon)\rho_F C_{PF}(T_m-T_R)-[1-(R/R_o)^3]\rho_F\Delta h_F-\varepsilon\rho_E h_E]\frac{\partial Y_m}{\partial t}$$
$$=-\left(K^*\frac{\partial T}{\partial x}\right)_{Y_m^+}\frac{\partial Y_m}{\partial x}+K_{MgO_S}\frac{\partial T}{\partial x}\bigg|_{Y_m^-}\frac{\partial Y_m}{\partial x}$$
$$+K^*\frac{\partial T}{\partial y}\bigg|_{Y_m^+}-K_{MgO_S}\frac{\partial T}{\partial y}\bigg|_{Y_m^-}. \quad \text{(B12)}$$

For one-dimensional penetration into MgO lining, the above equation simplifies to

$$\{\rho_{MgO_S}(h_{MgO_S}-h_E)+(1-\varepsilon)\rho_F[h_E-C_{PF}(T_m-T_R)]$$
$$-[1-(R/R_o)^3]\rho_F\Delta h_F\}\dot{Y}_m=K^*\frac{\partial T}{\partial y}\bigg|_{Y_m^+}-K_{MgO_S}\frac{\partial T}{\partial y}\bigg|_{Y_m^-}. \quad \text{(B13)}$$

EQUATIONS DU TRANSFERT DE CHALEUR ET DE MASSE DANS LES LITS POREUX GENERANT DE LA CHALEUR—II. FUSION PARTICULIERE ET PENETRATION DU SUBSTRAT PAR DISSOLUTION

Résumé—A l'assèchement du lit, les modes dominants du transfert thermique sont la conduction et le rayonnement. La rayonnement est schématisé par l'approximation de Rosseland. La fusion des particules d'acier inoxydable incrustées dans le combustible est modélisée en supposant que le lit est un continuum avec conduction et rayonnement comme mode dominant du transfert thermique. L'acier fondu, après son écoulement au fond du lit, est supposé disparaître dans des fissures et des joints de mortier entre les briques de MgO. La fusion du combustible à l'intérieur du lit est modélisée identiquement à celle des particules d'acier, excepté pour le lit. La couche fondue de combustible au fond du lit cause la surchauffe de MgO à la température de l'eutectique (2280°C) et le commencement de la dissolution de MgO conduit à la convection naturelle et au mélange dans la couche fondue. Les particules de combustible submergées commencement aussi à se dissoudre dans la solution fondue et cela conduit finalement à la conversion des débris en un bain fondu de combustible et de MgO. Lorsque le bain fondu atteint un état gelé ou de repos, l'épaisseur de l'alignement de briques en MgO est estimée 'sûre' pour un lit donné et un flux externe de refroidissement fixé.

GLEICHUNGEN FÜR DEN WÄRME- UND STOFFÜBERGANG IN WÄRMEFREISETZENDEN PORÖSEN SCHÜTTUNGEN—II. SCHMELZ- UND AUFLÖSUNGS-VORGÄNGE

Zusammenfassung—Bis zum Austrocknen der Schüttung wird die Wärmeübertragung von der Wärmeleitung und der Strahlung bestimmt. Für die Strahlung wird ein Ansatz nach Rosseland verwendet. Der Schmelzvorgang des rostfreien Stahles, der teilweise im Brennstoff eingebettet ist, wird mit Hilfe der Annahme dargestellt, daß die Schüttung ein Kontinuum sei, in dem Leitung und Strahlung die wesentlichen Arten der Wärmeübertragung sind. Es wird weiter angenommen, daß der geschmolzene Stahl, nachdem er auf den Grund der Schüttung getropft ist, in Ritzen und Fugen der Mg0-Auskleidung verschwindet. Das Schmelzen des Brennstoffes geht in ähnlicher Weise vonstatten wie beim Stahl. Die Brennstoffschmelze führt zum Aufheizen der Mg0-Auskleidung bis zur eutektischen Temperatur (2280°C), dadurch beginnt sich die Mg0-Auskleidung aufzulösen. Das führt infolge des Dichteunterschieds zwischen Mg0 und Brennstoffschmelze zu freier Konvektion und zur Durchmischung der Schmelze, wobei schließlich die gesamten Trümmer eingeschmolzen werden. Der Prozeß des Einbrandes der Mg0-Auskleidung erfolgt solange, bis die Konzentration des Brennstoffs im Schmelzbad (infolge des Mischprozesses) soweit erniedrigt wird, daß die volumenbezogene Wärmeerzeugung zu gering ist, um das Schmelzbad flüssig zu erhalten.

УРАВНЕНИЯ ТЕПЛО- И МАССОПЕРЕНОСА В ТЕПЛОВЫДЕЛЯЮЩИХ ПОРИСТЫХ СЛОЯХ—II. ПЛАВЛЕНИЕ ЧАСТИЦЫ И ПЕРЕНОС ВЕЩЕСТВА ПРИ РАСТВОРЕНИИ

Аннотация—Основными механизмами теплопереноса в слое являются теплопроводность и излучение. Перенос излучением описывается в приближении Росселанда. Плавление частицы из нержавеющей стали, находящейся в слое топлива, моделируется в предположении, что слой безграничен, а теплопроводность и излучение определяют перенос тепла. Предполагаем, что расплавленная сталь после ее стекания на дно, исчезает в трещинах и соединительных швах кирпичей из MgO. Плавление частицы топлива внутри слоя моделируется аналогично плавлению частицы стали, за исключением явления его оседания, более явно выраженное в случае плавления топлива, и которое предполагаем мгновенным из-за значительного веса расположенного сверху слоя и натриевого охладителя. Расплавленный слой топлива по мере его накопления на дне вызывает разогрев облицовки из MgO до температуры эвтектики (2280°C) и она начинает растворяться. Градиент плотности, возникший из-за растворения MgO, приводит к естественной конвекции и перемешиванию расплавленного слоя. Частица топлива также начинает растворяться в расплаве, состоящей из топлива и MgO, и в конце концов исчезает в нем. Проникновение MgO продолжается до тех пор, пока процесс перемешивания понижает концентрацию топлива в объеме до уровня, при котором скорость внутреннего тепловыделения на единицу объема недостаточна для поддержания защитной оболочки в расплавленном состоянии, и приводит к ее затвердеванию. В этом случае предполагается, что предусмотренная толщина облицовки с помощью кирпичей из MgO является безопасной для заданной тепловой нагрузке слоя и скорости внешнего охлаждения.